Journal of Geodynamics 46 (2008) 78–89

Contents lists available at ScienceDirect

Journal of Geodynamics

journal homepage: http://www.elsevier.com/locate/jog

Earth tides observed by gravity and GPS in southeastern Alaska

T. Sato[a,*], S. Miura[a], Y. Ohta[a], H. Fujimoto[a], W. Sun[b], C.F. Larsen[c], M. Heavner[d], A.M. Kaufman[c], J.T. Freymueller[c]

[a] *Research Center for Prediction of Earthquakes and Volcanic Eruptions, Graduate School of Science, Tohoku University, 6-6 Aza-Aoba, Aramaki, Aoba-ku, Sendai, Miyagi 980-8578, Japan*
[b] *Earthquake Research Institute, University of Tokyo, Tokyo, Japan*
[c] *University of Alaska, Fairbanks, USA*
[d] *University of Alaska Southeast, Juneau, USA*

ARTICLE INFO

Article history:
Received 6 September 2007
Received in revised form 20 March 2008
Accepted 27 March 2008

Keywords:
Southeastern Alaska
Gravity tide
Tidal displacement
Oceanic tidal effect
Regional ocean tide model
PPP method

ABSTRACT

We analyzed gravity data obtained in Juneau and global positioning system (GPS) data obtained from three PBO sites in southeastern Alaska (SE-AK), which are part of a US research facility called 'EarthScope', and we compared the obtained tidal amplitudes and phases with those estimated from the predicted tides including both effects of the body tide and ocean tide. Global tide models predict the ocean tides in this region of complex coastline and bathymetry. To improve the accuracy of prediction, we developed a regional ocean tide model in SE-AK.

Our comparison results suggest: (1) by taking into account the ocean tide effect, the amplitude differences between the observation and the predicted body tide is remarkably reduced for both the gravity and displacement (e.g. for the M_2 constituent, 8.5–0.3 μGal, and 2.4–0.1 cm at the AB50 GPS site in Juneau in terms of the vector sum of three components of the north–south, east–west and up–down), even though the ocean tide loading is large in SE-AK. (2) We have confirmed the precise point positioning (PPP) method, which was used to extract the tidal signals from the original GPS time series, works well to recover the tidal signals. Although the GPS analysis results still contain noise due to the atmosphere and multipath, we may conclude that the GPS observation surely detects the tidal signals with the sub-centimeter accuracy or better for some of the tidal constituents. (3) In order to increase the accuracy of the tidal prediction in SE-AK, it is indispensable to improve the regional ocean tide model developed in this study, especially for the phase.

1. Introduction

Southeastern Alaska (SE-AK) is a region with very rapid uplift rates, exceeding 30 mm/year in maximum, which are mainly caused by glacial isostatic adjustment (GIA), including the effects of past and present-day ice melting (Larsen et al., 2005, 2007). A joint Japanese–American observation project called International geodetic project southeastern Alaska (ISEA) was initiated in 2005 to follow up the work of the University of Alaska Fairbanks (UAF) by adding new geodetic data sets (Miura et al., 2007). In this project, three kinds of geodetic measurements are carried out to study GIA, loading deformation, and tidal variations in and around Glacier Bay in SE-AK: (1) the absolute gravity (AG) and relative gravity surveys, (2) surveys with global positioning system (GPS) and the establishment of new continuous GPS sites and (3) gravity tide observations. We also make use of EarthScope continuous GPS data.

The tides, including the oceanic tidal loading (OTL) effects, are the major signal in these geodetic observations over periods less than seasonal. For example, the magnitude of residual time series of our AG measurements in SE-AK after correcting for the effects of body tide (not shown here) are about 30 μGal (1 μGal = 1 nm s^{-2}) in the peak-to-peak amplitude, and the main part of these residuals is due to the effects of OTL. The OTL effect is 15–30 times larger than the nominal precision of the absolute gravity measurements (i.e. 1–2 μGal). Therefore, precise estimation of the ocean tide effects (i.e. the effects of attraction and loading) is indispensable to increase the accuracy of gravity and GPS observations made to study GIA, especially AG measurements, when they are carried out over a short period.

SE-AK and Northwest British Columbia shows large ocean tide amplitude. For example, in Juneau, the total tidal range is about 8 m (NOAA website, http://tidesandcurrents.noaa.gov/index.shtml). Lambert et al. (1998) intensively studied the OTL effects on gravity and displacement around the Canadian coasts including the Western Coast of Canada based on both the global ocean tide models (i.e. they used two models of Schwiderski, 1980; Le Provost et al., 1994) and the regional ocean tide models developed by their

* Corresponding author. Fax: +81 22 264 3292.
E-mail address: tsato@aob.geophys.tohoku.ac.jp (T. Sato).

0264-3707/$ – see front matter © 2008 Elsevier Ltd. All rights reserved.
doi:10.1016/j.jog.2008.03.004

group. They demonstrated a significant reduction in the variances of both the residuals of the AG and GPS measurements at the most sites in the Western Canada by correcting for the OTL effects. They also pointed out the importance of improvement of regional ocean tide loading models to realize the sub-centimeter precision for both the gravity and position measurements over period shorter than 1 day. Schenewerk et al. (2001) investigated the vertical OTL displacements for eight major tidal constituents at 353 permanent GPS sites distributed around the world. Their results indicate that, in general, estimates for the sites at high latitudes or in regions with complex coastlines are less accurate than those in other places, probably because of limitations in the ocean tide models in such places. For example, the sites located on the Gulf of Alaska coast show the OTL signals of 3–5 cm in amplitude and the discrepancy between the observed OTL effects and the model predictions are at the order of 1–2.4 cm. A global ocean tide model by Schwiderski (1980) was used for their study.

Thanks to the satellite sea surface altimeters such as TOPEX/Poseidon and Jason-1, the accuracy of the recent global ocean tide models has been much improved compared with those in the 1980s, and consequently the accuracy of estimation of loading effect has been remarkably improved (e.g. Bos et al., 2002; Sato et al., 2004; Neumeyer et al., 2005). On the other hand, they pointed out importance to take into account tide gauge measurements for the ocean loading correction for the gravity stations near the coasts. From GPS data for two sites in Alaska (Chi3 and Fairbanks, north of our study area), Khan and Tscherning (2001) estimated OTL displacements for the semi-diurnal components, confirming large OTL signals that were not accurately predicted by global models. As shown later, in SE-AK, we observe large discrepancies among the proposed global ocean tide models. Therefore, in order to improve the accuracy of the correction for the OTL effects on our geodetic observations, we have developed a new regional ocean tide model for SE-AK. To access the accuracy of the predicted earth tides based on this ocean tide model, we compared them to the gravity and GPS observations. To compute the regional ocean tide model, we took into account the tide gauge data obtained in the SE-AK region.

Fig. 1 shows the map of the study area, the locations of the tide gauge stations and the gravity and GPS sites related to this study.

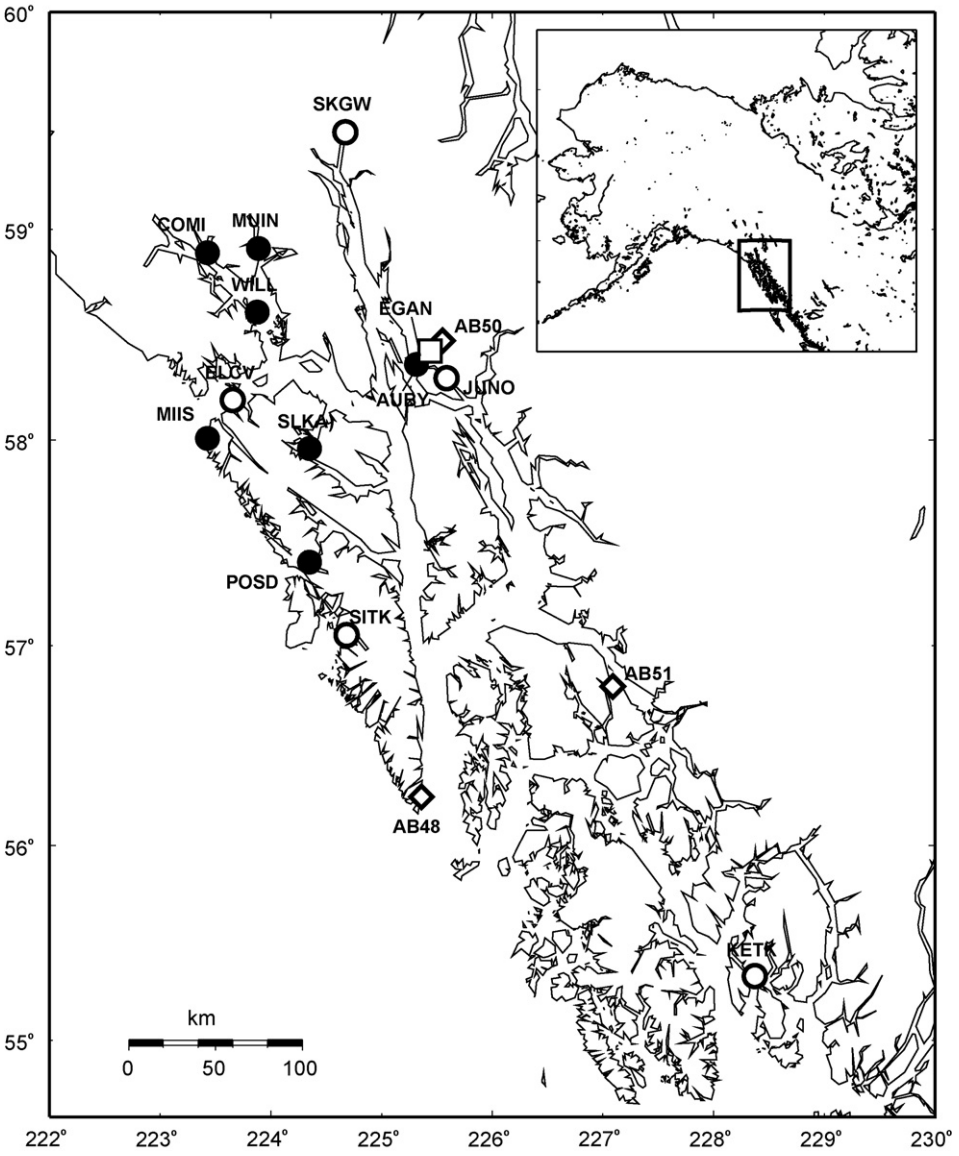

Fig. 1. Locations of the observation sites used in this study. Details of each site are listed in Table 1. An open square, a diamond, open circles, and closed circles indicate the tidal gravity, continuous GPS, continuous tide gauges, and temporal tide gauges installed by UAF (Larsen, 2003), respectively.

Table 1
Station list used in this study

Code	Station name	Longitude	Latitude	Note
EGAN	Eegan libraly of UAS	225.360E	58.385N	Gravimeter of TU
AB48	Port Alexander	225.353E	56.245N	PBO GPS site
AB50	Mendenhall Glacier Visitor Center	225.455E	58.417N	PBO GPS site
AB51	Petersburg	227.086E	56.797N	PBO GPS site
ELCV	Elfin Cove	223.657E	58.193N	CTG of NOAA
JUNO	Juneau	225.588E	58.298N	CTG of NOAA
KETK	Ketchikan	228.375E	55.333N	CTG of NOAA
SITK	Sitka	224.658E	57.052N	CTG of NOAA
SKGW	Skagway	224.673E	59.450N	CTG of NOAA
AUBY	Auke Bay	225.350N	58.385N	TTG of UAF
COMI	Composit island	224.43E	58.89N	TTG of UAF
MIIS	Miner Island	223.66E	58.00N	TTG of UAF
MUIN	Muir Inlet	223.89E	58.90N	TTG of UAF
POSD	Point Sinbad	224.35E	57.41N	TTG of UAF
SLKA	Salt Lake	224.34E	57.96N	TTG of UAF
WILL	Willoughby	223.88E	58.61N	TTG of UAF

Note: TU, Tohoku University, Japan; UAF, University of Alaska, Fairbanks; UAS, University of Alaska, Southeast; NOAA, National Oceanic and Atmospheric Administration of USA; PBO, Plate Boundary Observatory; CTG, continuous tide gauge stations operated by NOAA; TTG, Temporal tide gauge station installed by Larsen (2003).

The coordinates of these stations and the data sources are listed in Table 1.

Since the late 1990s, GPS has been widely used to study OTL (e.g. Schenewerk et al., 2001; Allinson et al., 2004; Thomas et al., 2007). Allinson et al. (2004), who analyzed the GPS data more than 1000 days in length, showed that estimates of OTL effects at the principal semi-diurnal and diurnal tidal frequencies were well resolved by the PPP method. On the other hand, King (2006) compared tidal loading displacement estimates using both the kinematic and static methods based on the GPS data collected during 5 years at the South Pole. They suggested that the accuracy of kinematic estimates is lower than the static estimates and the height time series is dominated by non-tidal effect.

We applied here a kinematic PPP method to extract the tidal signals from the time series of GPS coordinates. Many of the previous studies indicate biases in estimates of the K_1 tidal signals due to an alisasing effect between the GPS satellite orbits and related signals (e.g. Hatanaka et al., 2001; Schenewerk et al., 2001; King, 2006). Related to the OTL correction for the GPS data analysis, Dragert et al. (2000), who studied the GPS data obtained at a coastal site in the western Canada (Holberg), reported that, for the daily solutions without the OTL corrections, the significant amount of the relative vertical station motion was absorbed in their 1-h tropospheric delay estimates. We also investigate these errors mentioned above in our GPS analysis for SE-AK.

2. Gravity data and processing

The gravity data used in this study were obtained from a Scintrex CG-3M AUTOGRAV gravimeter set at the Egan library of the University of Alaska, Southeast (UAS) in Juneau (station coordinates: 58.3354N, 225.3600E, 38 m). The data were sampled at 1-s intervals and they were directly transferred to Tohoku University via Internet. For the tidal analysis, the 1-s data were decimated to the interval of 1-h by two steps: (1) sampling of the 1-second data at every 1 min using a 250 s low-pass filter (LPF) and (2) sampling of the filtered 1-min data at every 1 h using a LPF of 361 in the number of filter weights.

The original data show a large drift with an almost constant rate of about −110 μGal/day over the whole observation period and they include large step-like jumps due to the automatic resetting by a built-in function of the gravimeter. Before the tidal analysis, we corrected the drift by fitting a linear function to each data segment divided by the jumps, and the steps were corrected based on the differences between the constant parts obtained from the linear fitting. The 1-h data include a spike-change due to the effects of earthquakes and the maintenance works of the gravimeter. As will be described in Section 4, we rejected such bad data from the tidal analysis.

We analyzed the gravity data obtained over 1 year from 16 June 2006 to 14 June 2007. As an example of the tidal analysis, Fig. 2 shows the data of about 2 months in length, which a linear drift was extracted. From the top, the original data, the short-period tides, the trend including the long-period tides and the irregular part are displayed. Seasonal variations are dominant signals in the trend component, which may be mainly caused by the effect of temperature changes at the gravimeter room. Step-like change at

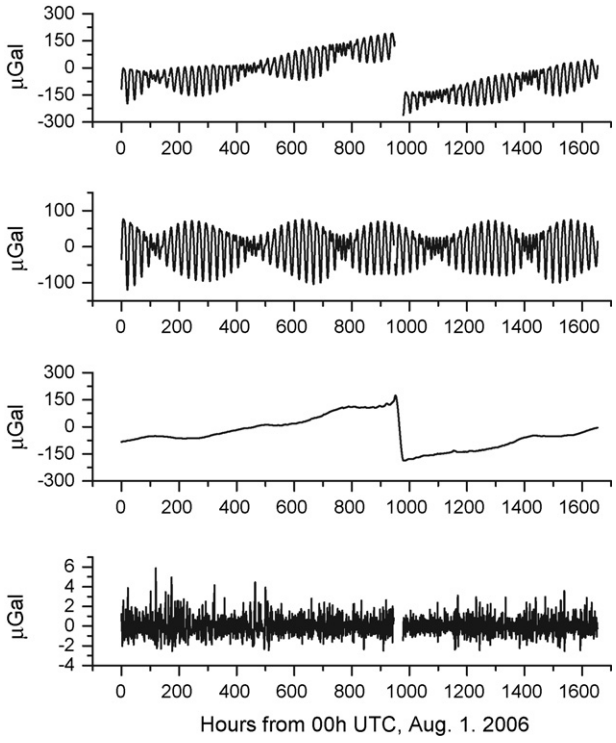

Fig. 2. Results of the gravity data decomposition at EGAN (see Fig. 1) obtained from the tidal analysis by BAYTAP-G (Tamura et al., 1991). From the top, the original 1-h sampled data, the decomposed tidal component, the trend component, and the residuals are shown.

Table 2
Strategy for the GPS data analysis

	Model/parameters
Site	Three of AB48, AB50 and AB51
Position	Lattitude: 58.417N, Longtitude: 225.440E
Obsercation window	31 h (3.5 h + 24 h + 3.5 h)
Observation time period	January 2006–June 2007
Elevation angle cut off	7°
Estimation intervals	300 s
Tropospheric mapping function	GMF (Boehm et al., 2006)
Satellite/receiver antenna phase center offset and variation	igs_05.atx (IGS absolute antenna PCV models)
Site displacement by earth tides	w/o correction
Reference frame	ITRF2000 (Altamimi et al., 2002)

around 950 h is an error in the correction for step mentioned above. As shown in the figure, they could be decomposed from the short-period tidal component by the tidal analysis, as explained in Section 4.

3. GPS data and processing

In this study, we used the GPS data obtained at three PBO continuous GPS sites, AB48, AB50 and AB51. PBO is part of a US research facility called EarthScope (http://earthscope.org). As shown in Fig. 1, AB48 faced the open sea and is located at the entrance of a long strait (Chatham Strait). AB50 is located adjacent to both our tidal gravity station and the AG sites in Juneau. AB51 is located in Petersburg, where, as shown later, the M_2 ocean tide shows a large amplitude exceeding 3 m. For each site, the data used for the analysis was 1.5 years in length (January 2006–June 2007).

To estimate the tidal displacement, we used a PPP method, which was initially introduced by Zumberge et al. (1997). The software used here is 'GpsTools ver. 0.6.3' (Takasu and Kasai, 2005; Takasu, 2006), which is a GPS/Global Navigation Satellite System (GNSS) analysis software package. To apply the PPP method to our data, we used the International GNSS Service (IGS) precise orbits and clock information referred to the satellite coordinates and clock correction. The time-dependent unknown parameters were estimated for each time window of 31 h in length by using the extended Kalman filter (EKF, forward/backward) and fixed interval smoother. Moreover, the GPS receiver coordinates were estimated using a random-walk stochastic model every 5 min without earth tides correction.

The window length of 31 h was selected to reduce the possible artificial edge effect of Kalman filtering in the end of each day, because there are no tidal harmonics corresponding to the period of 31 h. Successive time windows overlapped each other by 3.5 h. The tropospheric zenith total delay (ZTD) at the GPS site was estimated at every 5 min assuming random-walk model with sigma of $1 \times 10^{-4}\,\mathrm{m^1\,s^{-1/2}}$. The horizontal tropospheric gradient also estimated at every 5 min assuming also a random-walk model with sigma of $1 \times 10^{-5}\,\mathrm{m^1\,s^{-1/2}}$ at quadratic form. Carrier phase ambiguities were not resolved because the current version of GpsTools does not implement that capability.

Table 2 gives a summary of the GPS analysis strategy and related information. An example time series is shown in Fig. 3. In this figure, we observe that the tidal variations are clearly reproduced by the kinematic PPP method, and it is the major signal in the time series.

4. Tidal analysis

The analysis was performed using the BAYTAP-G tidal analysis program (Tamura et al., 1991). Using this code, we decomposed

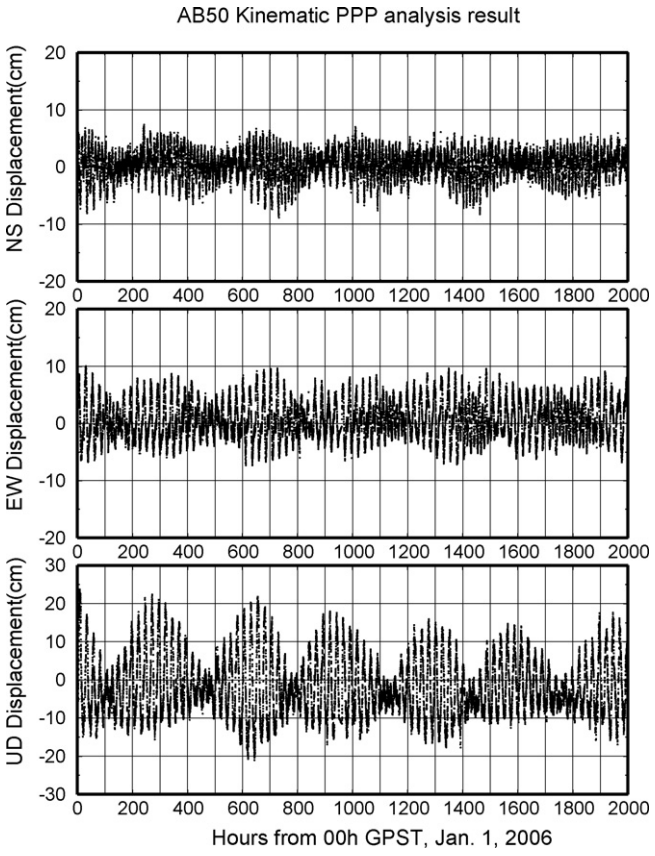

Fig. 3. Example of a time series of station coordinates at AB50 (see Fig. 1) obtained by the PPP method (Takasu and Kasai, 2005 and Takasu, 2006). The data for 1 January to 25 March 2006 are displayed. From the top, the northward (NS), eastward (EW), and upward (UD) components are shown in cm. Horizontal axis is in GPS time (GPST).

both the gravity and GPS data into three components: the tide, the trend and the irregular residuals. The BAYTAP-G program tries to discriminate the trend component by fitting an integrated random walk model. As shown in Fig. 2, this algorithm generally works well to decompose the tidal component from the original data including the trend component, which is not easy to represent with a low-order polynomial. The random walk model was also used in the PPP analysis for the GPS data to decompose the tidal component.

To determine the mean values of tidal amplitude and phase as precisely as possible, we rejected irregular data such as spike-like noise due to the earthquakes and the maintenance work of the gravimeter, because these noises easily disturb the estimated amplitudes and phases by spreading noise over wide frequency band. To avoid this, using a built-in function of BAYTAP-G, we rejected the bad data from the tidal analysis that showed residuals exceeding 3-sigma of the standard deviation of the decomposed irregular part. This method was applied to the analysis for both the gravity and GPS data.

The analysis results are shown in Table 3. In this table, the phase means the local phase and phase lag is represented with plus sign. Root mean square errors are estimated based on the standard deviations of the residuals.

5. Modeling of the regional ocean tide in SE-AK

5.1. Accuracy of global ocean tide models in SE-AK

The accuracy of the recent global ocean tide models is high, except for shallow seas and/or for sea areas having complex

Table 3
Tidal analysis results for the gravity data at EGAN and the GPS data at three sites of AB48, AB50 and AB51

Site	O_1		K_1		M_2		S_2	
	Amp.	Phase	Amp.	Phase	Amp.	Phase	Amp.	Phase
Gravity								
EGAN	33.29 ± 0.13	−4.21 ± 0.22	47.05 ± 0.12	−4.15 ± 0.15	15.56 ± 0.05	−4.07 ± 0.17	9.34 ± 0.04	−12.08 ± 0.27
GPS								
AB48	6.48 ± 0.06	10.51 ± 1.07	8.32 ± 0.06	16.72 ± 0.67	3.50 ± 0.07	7.47 ± 3.70	1.99 ± 0.07	19.16 ± 2.52
AB50	6.04 ± 0.11	6.34 ± 3.34	7.35 ± 0.10	13.65 ± 1.77	3.74 ± 0.05	8.07 ± 1.00	2.16 ± 0.05	28.87 ± 1.41
AB51	6.31 ± 0.03	7.73 ± 0.55	7.90 ± 0.04	10.18 ± 0.43	3.83 ± 0.04	8.86 ± 0.90	2.08 ± 0.04	19.61 ± 1.18

The displacements are shown with the vector sum of the NS, EW and UD components. Amp., amplitude in μGal and cm for the gravity and displacements, respectively. Phases, local phase lag.

bathymetry and coastline as SE-AK. For example, according to Matsumoto et al. (2000), the vector differences for the M_2 constituent between NAO.99b (Matsumoto et al., 2000) and GOT99.2b (Ray, 1999) are the order of 1 cm or smaller than it almost everywhere in the open seas in the world. Matsumoto et al. (2006) compared the recent global ocean tide models with the actual ocean bottom pressure gauge (OBPG) measurements in the western Pacific off Sanriku in northern Japan, and they conclude that the difference between the observation and the five global ocean tide models was less than 1.3 cm in terms of root sum square of the vector differences for eight major tidal constituents (i.e. Q_1, O_1, P_1, K_1, N_2, M_2, S_2, and K_2). The ocean models they compared are NAO.99 (an old version of NAO.99b), NAO.99b, GOT99.2b, CSR4.0 (Eanes and Bettadpur, 1994), and TPXO.6 (Egbert et al., 1994).

In contrast to the case for the open seas, the agreement among the above models is not so good in SE-AK. For example, at the grid points nearest to the Juneau tide gauge station (1.3–3.5° in angular distance away), the differences in the M_2 amplitude and phase are about 70 cm and 70° among the five global ocean tide models shown above. This is mainly due to a complex bathymetry and coastline. Therefore, in order to obtain a reliable ocean tide correction value, to improve the regional ocean tide model in SE-AK is indispensable.

5.2. Computational method

The computation was carried out with a simple method that integrates the simultaneous equations of the Navier–Stokes equation in a coordinate system rotating with the Earth and the equation of continuity (Fujii, 1967). The area of the model is 5.6° by 7.1° in latitude and longitude, respectively, i.e. 54.5N to 60.1N and 221.9E to 230.0E. The topography and bathymetry are modeled based on the ETOPO2 bathymetry data with the spatial resolution of 2 min by 2 min (http://www.ngdc.noaa.gov/mgg/fliers/01mgg04.html).

The model was driven by giving the time variations in the tidal height on the boundary lines at the west and south edges of the model. We used here the NAO.99b model (Matsumoto et al., 2000) for the boundary values. This model was generated by hydro-dynamically assimilating the TOPEX/Poseidon sea surface altimeter data over the whole oceans in the world. We also took into account the tide gauge data at 12 stations available in the study area, five NOAA continuous tide stations and seven of temporary sites installed by UAF (Larsen, 2003). Their locations and the coordinates are shown in Fig. 1 and Table 1.

The time step used for the integration was 6 s. The spin up time with this time step was about 1.5 days for the M_2 wave and it was also similar to the diurnal waves. To reduce a possible nonlinear effect due to the shallow depth in the coastal regions, we artificially set the minimum sea depth to 20 m. Other adjustable parameters to be considered are the coefficients for the bottom friction, the horizontal mixing and the non-linear term.

5.3. Computational results

The computation is sensitive to the assumed magnitude of the bottom friction (BF). We have searched for the best value in our model computation by changing the BF value within the range of 0.0001–0.1 (here the unit of the coefficient is given in the CGS system). Fig. 4 shows an example of the test results for the M_2 constituent at two grids which are at Elfin Cove (the entrance of a bay) and Juneau (the back of it), respectively (see Fig. 1). This figure plots the differences between the amplitudes computed without the tide gauge data and those observed at the respective two locations. So, we may expect that the best BF value should give the amplitude close to the observed one.

As shown in Fig. 4, the best BF values are slightly different at each site mainly due to the difference in the geographical condition. However, the difference in the best BF is not so large comparing the range of amplitudes obtained by changing the BF coefficients by the three orders tested here. Therefore, we used here the average value for these two sites (i.e. 2.9×10^{-3}) over the whole sea area of the model considered here. We also tested the BF values for the K_1 constituent which has the major amplitude in the diurnal tide. Different from the case of the M_2 constituent, the peak of the curve for the K_1 constituent was broad suggesting that the K_1 wave is not so sensitive to the assumed BF values.

Fig. 5(a) and (b) shows the distribution of the M_2 amplitude and phase, which were obtained by assuming the coefficients of 2.9×10^{-3}, 2.55×10^{-5} and 1.0×10^{-3} in unit of the CGS system for the bottom friction, the horizontal mixing and the non-linear term, respectively, and taking into account the data from 12 tide

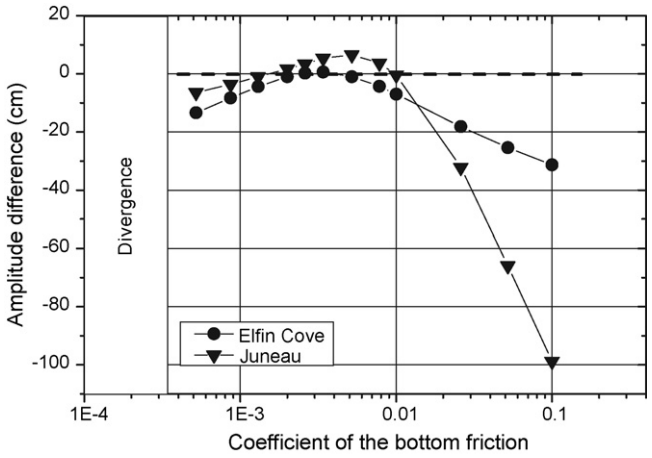

Fig. 4. Change in the amplitude difference between the observed M_2 constituent and the computed one by changing the coefficients of bottom friction. Circles and triangles correspond to two tide gauge sites at Elfin Cove and Juneau, respectively.

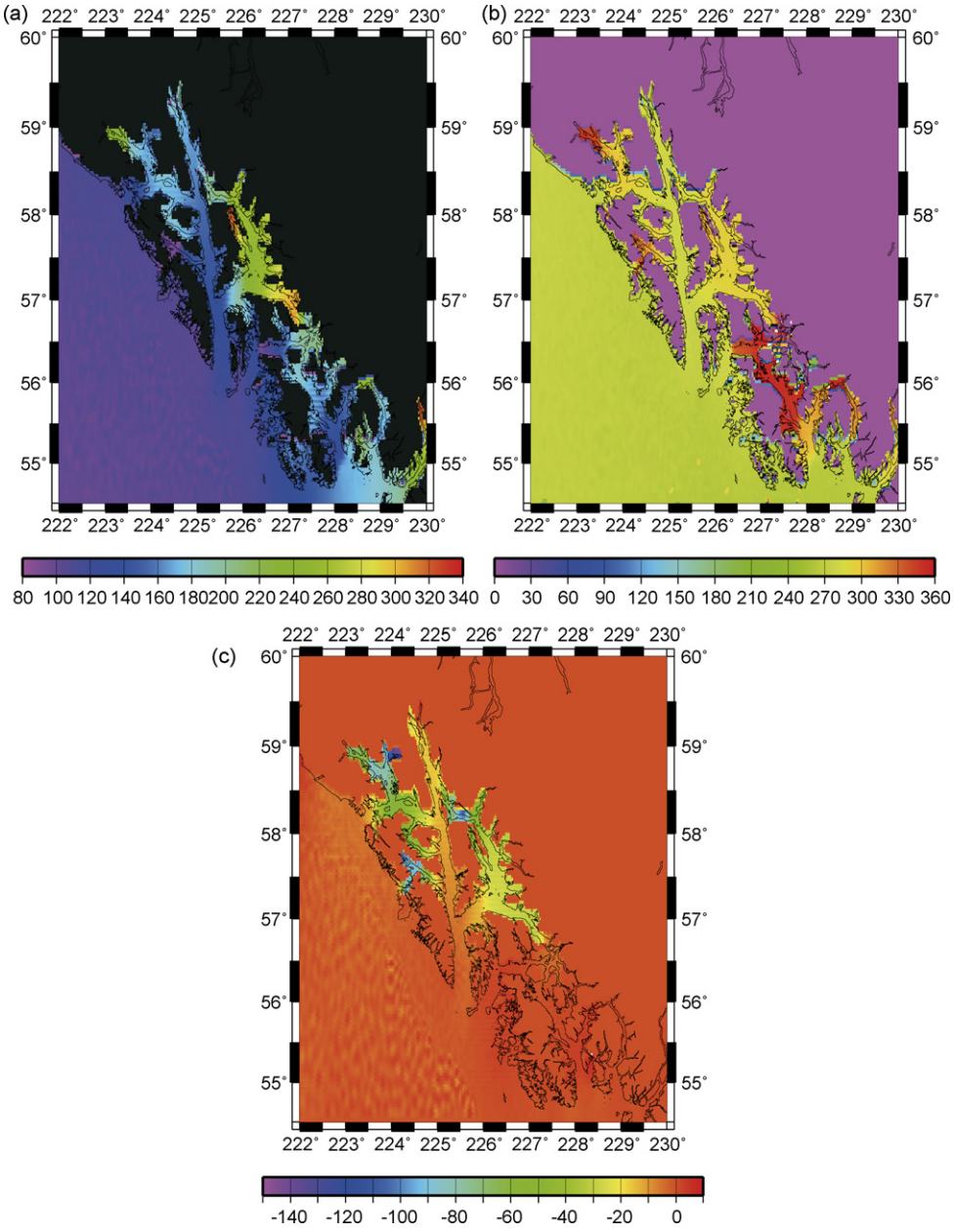

Fig. 5. Computed regional ocean tide model for the M_2 constituent and the amplitude difference between two models of A and B (Model A and Model B). Whereas both are regional ocean tide models based on the NAO.99b global ocean tide model (Matsumoto et al., 2000), Model A was computed without the observed tide gauge data, while Model B includes them. (a) The amplitude distribution of Model B in cm, (b) the local phase of Model B in degrees, and (c) distribution of the amplitude difference between Models A and B, where the color scale denotes 'A minus B'.

gauges shown in Fig. 1. We can observe a general tendency that the amplitude grows and the phase is delayed toward the back of the bays, channels, or fjords. The maximum amplitude reaches ~340 cm around the area of 56.8N and 227.3E, where the three channels of Frederick Sound, Sumner Strait and Clarence Strait meet together. Around Juneau (58.4N and 225.4E), the area with the M2 amplitude of 140–200 cm extends as expected from the observation.

To examine the effects of the tide gauge data on our modeling in SE-AK, we compared two cases. One does not use the tide gauge data (Model A) and other uses them (Model B). Fig. 5(c) shows the distribution of the amplitude difference between Model A and Model B (i.e. B minus A). As shown in Fig. 5(c), in general, the amplitudes of Model A are larger than Model B. The areas showing difference exceeding 100 cm at around Juneau and over the Glacier Bay region. However, the large amplitude in Model A is suppressed in Model B by introducing the actual tide gauge data into the model computation, as shown in Fig. 5(a).

6. Prediction of the tidal effects

6.1. Ocean tide effects

Based on the NAO.99b global ocean tide model (Matsumoto et al., 2000) and the regional model described in Section 5, we have estimated the OTL effects on the gravity and GPS observations. Following Farrell (1972) Farrell's method (1972), we estimated the

ocean tide effects by convolving, respectively, the cosine and sine amplitudes with the Green's function of loading over the whole oceans in the world. For the Green's function, we used the PREM earth model (Dziwonski and Anderson, 1981). The computation was performed using a code modified from the computer program 'GOTIC' by Sato and Hanada (1984). The main modification of the program was for the part related to the grid system to represent the topography because all of the observation sites used here are located very close to the seacoast (i.e. for example, about 450 m for EGAN and about 7 km for AB50).

The convolution result is sensitive to the accuracy of the topographic map used for land-sea masking, especially in the attraction part of the gravity effect. To represent the topography around the observation sites accurately, we used five kinds of the topographic maps with different grid intervals. We call here them as the 1st-, 2nd-, 3rd-, 4th- and 5th-order grids. The 5th-order grid was used for the computation of the gravity effect at EGAN, and its size is 5 by 10 in arc-seconds in latitudinal and longitudinal directions (i.e. about 154 m by 162 m in the respective directions). The land–sea distribution inside the area of the regional ocean tide models was represented with the 3rd-, 4th-, and 5th-order grids. The grid sizes of 3rd- and 4th-order are 2 by 2 in min of ETOPO2 (http://www.ngdc.noaa.gov/mgg/fliers/01mgg04.html) and 0.5 min by 1.0 min. In the remaining two areas of the 1st- and 2nd-order grids, the original NAO.99b model of 0.5° by 0.5° and ETOPO5 (the same web site as ETOPO2) of 5 min by 5 min were used.

In our case, for example, the gravity contribution (attraction plus loading) from the sea area representing with the regional ocean tide model (excluding the area represented with 5th-order grid) is about 5.5 μGal for the M_2 constituent at EGAN and it is about 60% in magnitude of the total effect that was integrated over the whole oceans in the world. The contribution from the sea area using the 5th-order grid (3 min by 6 min in the size of the area) is about 1.7 μGal.

6.2. Prediction and observation

We compared here predicted tides consisting of the body tide and the OTL effects to observations. For the body tide, we tested three tidal factors. One is given by Wahr (1981) for the 1066A earth model (Gilbert and Dziewonski, 1975) and other two are given by Dehant et al. (1999) for the PREM model (Dziwonski and Anderson, 1981), that is, one for the elastic and hydrostatic (EL-HY) earth and one for the inelastic and non-hydrostatic (IE-NH) earth.

Although the amplitude differences among the three models are not so large, the differences between the Wahr model and the DDW_IE-NH model are relatively large for gravity. They are 0.439, 0.205, 0.283 and 0.205 in unit of μGal for the M_2, S_2, K_1 and O_1 constituents at EGAN. This may be due to differences in the definition of latitude dependency of the tidal factor, as pointed out by DDW (1999). On the other hand, for displacement, the differences are relatively large between the DDW_EL-HY model and the DDW_IE-NH. For example, at AB50, differences in terms of the vector sum of NS, EW and UD are 0.10 cm, 0.04 cm, 0.13 cm, and 0.10 cm for the respective constituents mentioned above. In both the gravity and displacement, the differences of the estimated body tides are similar in magnitude to the observed amplitude errors shown in Table 3. For the M_2 constituent, the differences of the estimated body tides are rather large compared with the observation errors. The K_1 constituent shows relatively large difference compared with other constituents. This is because of the effect of the resonance due to the free core nutation of the Earth's fluid core (e.g. DDW, 1999).

Fig. 6 shows the comparison of the predicted tides with the observations at four sites of EGAN for gravity and AB48, AB50 and AB51 for displacement. This 'phasor plot' represents the amplitude and phase with the polar coordinates taking the cosine-axis as *x*-axis and the sine-axis as *y*-axis. The phase lag is represented by the angle measured from the cosine-axis in the anti-clockwise direction. In this figure, the numbers shown, as BTA are the amplitude computed using the tidal factors for the DDW_EL-HY model. The phase lag of the body tides was assumed to be zero.

7. Discussion

7.1. Sensitivity to the ocean tide model

7.1.1. Global ocean tide model

To test the sensitivity of our predicted tides to the global ocean tide model, we compared the regional ocean tide models computed using the Schwiderski model (1980) and the FES2004 model (Lyard et al., 2006) for the boundary conditions, where, for FES2004, we used the averaged tidal heights over each grid of 0.5° by 0.5° along the boundaries. The tide gauge data were used in these models, as with Model B (Section 5.3). In this comparison, the predicted tides were computed with the DDW_EL-HY tidal factor and the Green's function for PREM.

Table 4 compares results for the M_2 constituent at EGAN for the gravity and the UD component at three GPS sites for the same constituent, which shows the largest OTL effect among three components of NS, EW and UD. We observe a systematic difference in both the amplitude and phase between the Schwiderski model and other two models. Thus, in general, the amplitudes predicted by the Schwiderski model are smaller than those by NAO.99b or FES2004. Phase lags predicted by the former model are also relatively small compared with the latter two models. However, the phase predictions made using the Schwiderski model are more consistent with the observations than those made using the more resent global models, for sites AB50 and AB51 located near the fjords and complex channels of SE-AK. For the site AB48, the phase difference among three ocean models is relatively small compared with that predicted at AB50 and 51. For gravity at EGAN, all the model predictions are similar to the observations, suggesting the contribution of the tide gauge data used in the boundary condition.

The comparison results shown here may indicate an error that comes from ignoring the correct hydrodynamics of the coastal region in SE-AK. The Schwiderski model was obtained by hydrodynamically extrapolating many tide gauge data from around the world. Four tide gauge data were used in the SE-AK region. Presumably, this may contribute to the better agreement in the comparison of phase in SE-AK, although, as indicated by the previous works shown in Section 1 (e.g. Bos et al., 2002; Sato et al., 2004; Neumeyer et al., 2005) and described in Section 5.1, it is known that the recent tide models based on the satellite altimeter data should give the amplitude and phase better than those of Schwiderski model in the open seas.

7.1.2. Evaluation of the regional ocean tide model

We compared the predicted gravity and displacements by using Models A and B. The differences between Models A and B are much larger than the effect of changing the Earth's response, for most of the computations. However, in some cases, the differences between earth models are significant compared to the observation error, as described in Section 6.2.

For gravity, as shown in Fig. 6, Model B is remarkably consistent with the observed M_2 tide and the K_1 constituent is also improved relative to Model A. The actual tide gauge data at Juneau was used in Model B for one of the boundary conditions in the area around EGAN. This may contribute to the improvement. However,

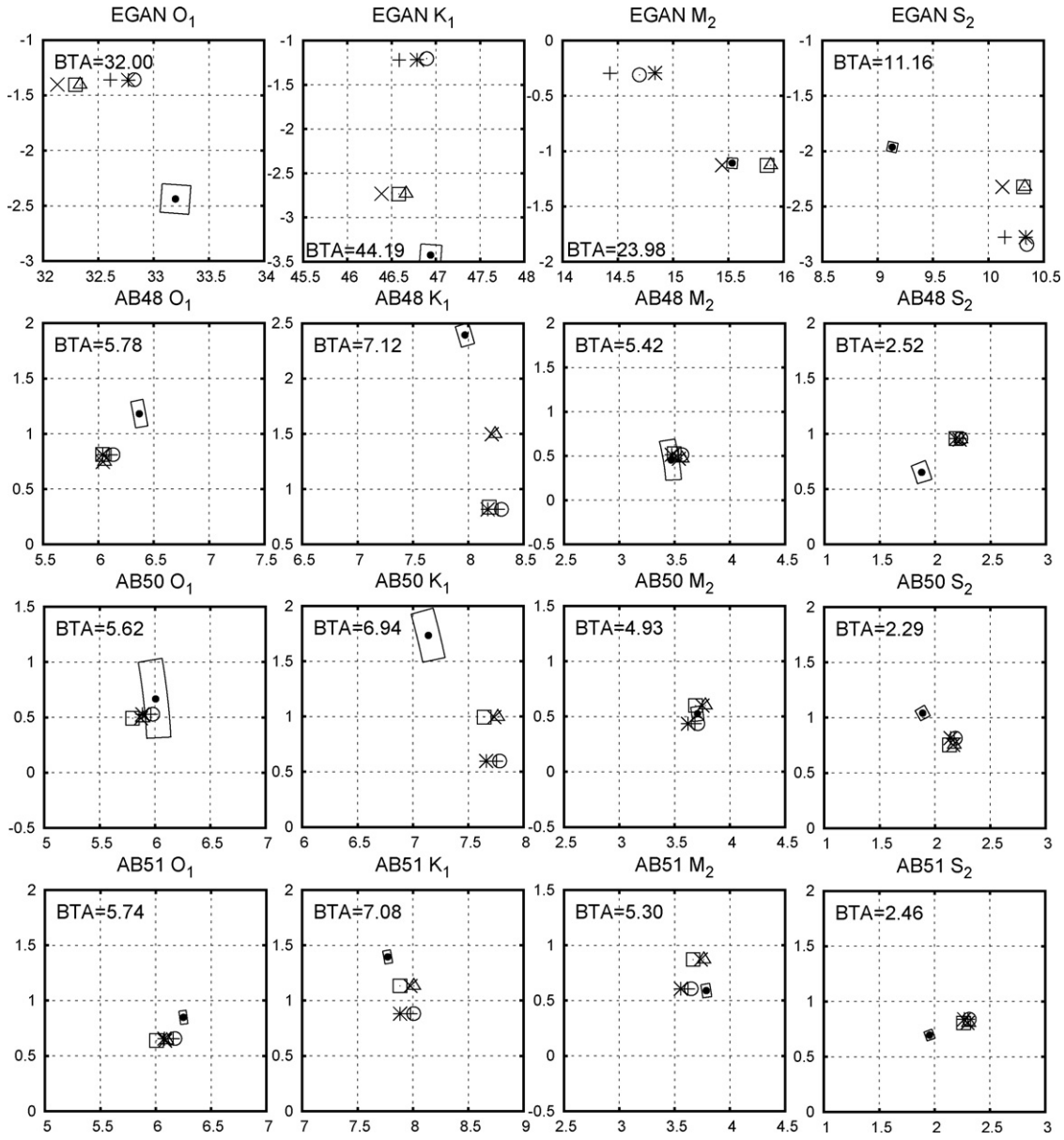

Fig. 6. Phasor plots for the observed and predicted tides at four sites of EGAN (gravity) and AB48, AB50, and AB51 (displacement). Units of both the horizontal and vertical axes are in μGal and cm for the gravity and displacement, respectively. For the displacement, the vector sums of three components of NS, EW and UD are plotted. The six kinds of prediction values are plotted in each figure, which were computed using different pair of the tidal factor and the ocean tide model (i.e. Model A or B). Three kinds of tidal factors are compared. One is by Wahr (1981) for the 1066A earth model (here WAHR), other two for the PREM earth model by DDW (1999), i.e. two of the elastic hydrostatic earth (DDW_EL_HY) and the inelastic and non-hydrostatic earth model (DDW_IE_NH). In each plot, the solid black circles are the observed values with the open sector that shows the observation error estimated by the BAYTAP-G tidal analysis and BTA shows the amplitude computed using the tidal factors for the DDW_EL-HY model. The phase lag of the body tides was assumed to be zero. The six combinations of the predicted body tide and the ocean tide model are plotted with the following symbols: (1) cross denoted with '+', predictions from WHAR and model A; (2) stars, DDW_EL_HY and model A; (3) open circle, DDW_IE_NH and model A, (4) Cross denoted with 'x', WAHR and model B; (5) open square, DDW_EL_HY and model B; (6) open triangle, DDW_IE_NH and model B.

for the S_2 and O_1 components, the improvement from including the tide gauge data is relatively small, even though the phase of S_2 is improved. We tested the atmospheric pressure effect on the observed S_2 tide by performing the BAYTAP-G analysis including the response to local air pressure data, and we obtained the amplitude and phase of 9.28 ± 0.05 μGal and $-12.07 \pm 0.28^\circ$, which are similar to the values shown in Table 3. For the O_1 constituent, the exact cause of the difference between the observation and the predictions is not clear at the moment.

For the displacement, Fig. 6 plots the vector sums of three components NS, EW, and UD. This figure indicates that, except for the K_1 constituent, agreement between the observations and the predictions is generally good in both the amplitude and phase at all the sites compared here. From Fig. 6, we also see that the differences between Models A and B are small compared with the difference in the gravity predictions. For gravity, the attraction part may contribute to the difference in sensitivity. In this connection, for the M_2 tides at the EGAN gravity site, which is located at about 7 km away from the AB50 GPS site, the amplitudes and phases of the attraction part are 3.35 μGal and 185.01° and 2.72 μGal and 185.44° for Models A and B, respectively. As shown in Fig. 6, for the M2 constituent, the difference between Models A and B is relatively large at AB51 compared with other sites. Large ocean tide amplitude exceeding 3 m may contribute to this.

Table 4
Result for the sensitivity tests of the predicted M_2 tide to the global ocean tide models and the comparison with the observations

Site	Model	Body tide		Oceanic effect		Total	
		Amp.	Phase	Amp.	Phase	Amp.	Phase
EGAN (Gravity)	OBS					15.57	−4.08
	SCH	23.97	0.00	9.00	185.19	15.03	−3.11
	NAO	23.97	0.00	8.20	187.90	15.89	−4.07
	FES	23.97	0.00	8.18	188.90	15.96	−4.78
AB48 (vertical displacement)	OBS					0.67	−11.51
	SHW	4.53	0.00	3.53	184.59	1.06	−15.51
	NAO	4.53	0.00	3.64	184.13	0.94	−16.13
	FES	4.53	0.00	3.48	184.92	1.11	−15.66
AB50 (vertical displacement)	OBS					1.65	−8.21
	SHW	4.03	0.00	2.52	185.11	1.54	−8.35
	NAO	4.03	0.00	2.53	190.09	1.60	−16.11
	FES	4.03	0.00	2.50	190.61	1.64	−16.29
AB51 (vertical displacement)	OBS					1.68	−12.24
	SHW	4.40	0.00	2.90	185.10	1.53	−9.69
	NAO	4.40	0.00	2.87	194.55	1.78	−23.84
	FES	4.40	0.00	2.77	195.37	1.87	−23.09

The regional ocean tide Model B (see section 6.1). For the prediction, the Green's function for the PREM earth model was used to compute the ocean tide effects and the tidal factors by DDW (1999) for the elastic and hydrodynamic PREM earth model, which is shown by DDW_EL_HY in Fig. 6 of this article. OGS, Observation; SCH, Schwderski model (Schwiderski, 1980); NAO, NAO.99b (Matsumoto et al., 2000); FES, FES2004 (Lyard et al., 2006)

7.1.3. Summary of the comparisons

As a summary of comparison results described in Sections 7.1.1 and 7.1.2, we may conclude that, by taking into account the ocean tide effect, the amplitude differences between the observation and the predicted body tide is remarkably reduced for both the gravity and displacement, even though the OTL effects are large in SE-AK and the ocean tides show complex spatial variations.

We extracted tidal signals from the time series of coordinates generated using the PPP method. Judging by the analysis errors shown in Table 3 and the comparisons shown in Fig. 6, we can say that PPP method works well to recover the tidal signals, except for the K_1 constituent. Table 5 shows the amplitude differences between the observations and the predictions that were obtained from the combination of the DDW_EL_HY, the Green's function for PREM, NAO.99b for the global model, and Model B for the regional model. This table indicates that, again except for the K_1 constituent, the observed tides could be recovered within the errors at the order of 0.1–0.5 cm for any constituents and at all sites compared here.

On the other hand, the sensitivity tests also indicate that our regional ocean tide model based on NAO.99b needs to be improved, especially for the phase. Tidal currents in SE-AK show very high speed and a complex pattern as suggested by observations in Glacier Bay (Cokelet et al., 2007) and as our model computations also suggest. To obtain a more reliable correction for the OTL effects, we need to improve our regional ocean tide models by using bathymetry data which are more accurate than those used in this study.

7.2. Tropospheric effects

It is known that, in GPS time series, the vertical coordinates are much noisier than the horizontal ones, mainly caused by the satellite constellation and by error in the wet zenith delay estimation. The similar situation is shown in Table 5, and the UD component shows larger observation errors and generally larger amplitude differences than the horizontal components. On the other hand, Table 5 indicates that, for the semi-diurnal tides, the amplitude difference of the vector sum is smaller than the UD component, and sometimes smaller than the NS and EW components. This means that the magnitude of the tidal displacement vector is deter-

Table 5
Amplitude differences between the observed tidal displacements from GPS and the predictions for the four constituents of O_1, K_1, M_2, and S_2

Site	Wave	Amplitude difference				Observation error			
		NS	EW	UD	VSM	NS	EW	UD	VSM
AB48	O_1	0.38	0.12	0.49	0.50	0.03	0.03	0.04	0.05
	K_1	0.50	0.89	1.43	1.57	0.03	0.03	0.05	0.06
	M_2	0.02	0.08	0.59	0.08	0.03	0.03	0.06	0.07
	S_2	0.38	0.24	0.82	0.43	0.03	0.03	0.05	0.07
AB50	O_1	0.10	0.14	0.24	0.27	0.02	0.10	0.03	0.11
	K_1	0.25	1.01	0.78	0.89	0.02	0.10	0.03	0.10
	M_2	0.11	0.10	0.23	0.08	0.02	0.03	0.04	0.05
	S_2	0.77	0.40	0.58	0.38	0.02	0.03	0.04	0.05
AB51									
	O_1	0.02	0.10	0.31	0.32	0.01	0.01	0.03	0.03
	K_1	0.23	0.34	0.25	0.29	0.02	0.02	0.03	0.04
	M_2	0.08	0.10	0.37	0.31	0.02	0.02	0.03	0.04
	S_2	0.27	0.25	0.54	0.33	0.02	0.02	0.03	0.04

In this table, the predicted tides were computed with the combination of the DDW_EL_HY, the Green's function for PREM, NAO.99b global tide model and the Model B regional tide model (see section 5.3). The results for three GPS sites of AB48, AB50 and AB51 are shown. Unit of the amplitude difference, cm. VSM, Vector sum of the NS, EW and UD components.

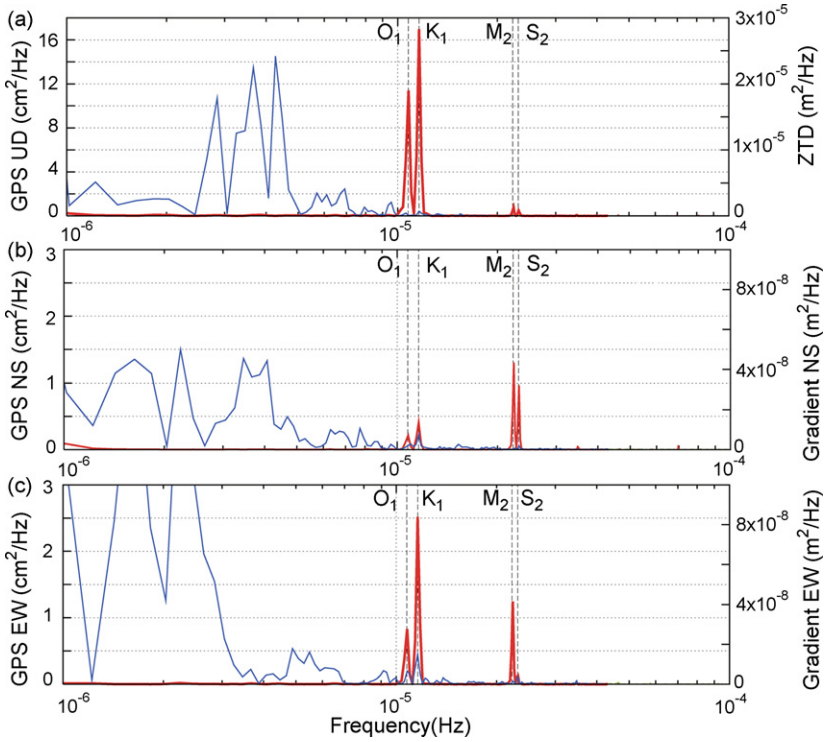

Fig. 7. Power spectrum density of the GPS-coordinate time series and related tropospheric parameters. (a) The GPS vertical and ZTD components. (b) Same as (a) but for the north-south component and north–south tropospheric gradient parameter. (c) Same as (a) but for the north–south component and north–south tropospheric gradient parameter. Red lines, PSD of the GPS coordinates; blue lines, PSD related the troposphere signals; black dashed lines, frequencies of O_1, K_1, M_2, and S_2 constituents.

mined more accurately than its orientation; the most likely cause for such an error is a small rotation of the tidal displacement vector due to correlations between the coordinate components. However, this tendency is not observed in the diurnal tides, suggesting that the observed diurnal tides of the horizontal components might be also affected by the tropospheric error much more than the semi-diurnal tides. King (2006) demonstrated that ambiguity fixing is a further avenue for improving the static technique since this will de-correlate the three coordinate components. In this analysis, we did not solve the carrier-phase ambiguities in the kinematic PPP approach (so-called "bias-free" solution).

The discrepancies in the K_1 constituent are larger than other constituents for any components of the coordinates and at all sites compared here, especially in the phase. As pointed out in previous studies (e.g. Schenewerk et al., 2001; Allinson et al., 2004), the K_1 constituent is very difficult to separate from multipath-bias and orbital error (Bock, 1991; Choi et al., 2004), as that period is nearly equal to the GPS satellite orbit repeat period. To examine the effect of trade-off between the obtained displacements and the tropospheric parameters in our GPS analysis, we compared the power spectrum density (PSD) between the GPS coordinate time series and tropospheric relation components (ZTD compared with the vertical displacement and the tropospheric gradient with the horizontal displacements). Fig. 7 shows the results for AB50, which has the fewest observation gaps among three sits used here. The data length used in the computation is 6 months, from 1 January 2006 to 30 July 2006. In this figure, the vertical dashed lines show the frequencies of O_1, K_1, M_2 and S_2 constituents.

As shown in Fig. 7, the dominant signals in troposphere relation components are observed in the frequency band of 10^{-6} to 10^{-5} Hz (several days in period), which may be related to the effects of meso-scale atmospheric motions. We also found clear peaks at the frequency of the K_1 constituent in all three components of the displacement, suggesting that the estimated K_1 signal possibly affected not only orbit and multi-path error but also ZTD and gradient estimation error. Vey et al. (2002) showed effect of OTL on GPS-derived ZTD estimates. They conclude that OTL effects translate into significant errors in ZTD estimates, with a scaling factor of 4.4 between ZTD and height for 10° elevation cut off angle. This means a 4.4-cm station height error would map into a 1.0-cm ZTD error. In this study, the maximum discrepancy of vertical component is 0.8 cm for the K_1 constituents in AB50, which results in a 0.16-cm ZTD error, or an ~0.3-mm error in precipitable water vapor (PWV). Nonetheless, ZTD estimation error and orbit repeating time origin errors should have some correlation. So, in this stage, we cannot distinguish these effects only from our data set.

Furthermore, we found small peak around the O_1 constituent, but it was slightly sifted from the exact frequency of the O_1 constituent. And also, there are not large peaks around semi-diurnal (M_2 and S_2) tidal biases compared with diurnal components except S_2 constituents in east–west component. These results conclude that our processing may affect ZTD and tropospheric gradient estimation error at diurnal constituents, especially K_1. In contrast, semi-diurnal constituents were basically resolved.

Last of this section, the atmospheric pressure (AP) changes may contribute to our analysis results for the GPS data as the changes in the AP loading (APL), especially for the vertical component. Although it is known that the major signal in APL is the seasonal one, sometimes, APL growths to the order of more than 0.5 cm in a few days (e.g. Manabe et al., 1991; Tregoning and van Dam, 2005). The PSDs of the GPS coordinates shown in Fig. 7 have a large power at the low frequency band, suggesting the contribution of effect of APL partly. For the further comparison and discussion of tidal displacements in SE-AK at the accuracy of sub-centimeter, we need to study not only the OTL effect but also the APL effect, especially for the long-period tide.

7.3. Gravity response to the tidal force and the OTL

The gravity effect of the loading tide at the EGAN site has a magnitude as large as 6 μGal for the M2 tide due to the large ocean tide amplitude, and it is about twice as large as the effect of attraction. We estimated effect of inelasticity on our gravity observation based on a complex Green's function for the inelastic earth given by Okubo and Tsuji (2001).

In their dynamic Green's function, the following three effects are taken into account: (1) the inertial term in the load Love/Shida numbers h', k' and l', (2) the inelasticity effect in the elastic constants inside the Earth, which is proportional to the inverse of Q-values for the bulk modulus and rigidity, where the Q-profile was taken from an absorption model given by Anderson and Given (1982), and (3) the effect of physical dispersion on the real part of the elastic constants referred to Smith and Dahlen (1981). In our computation, we used a Green's function based on the PREM model (Dziwonski and Anderson, 1981) and assuming 1/200 Hz as the reference frequency and $\alpha = 0.15$ (a coefficient to represent the frequency dependency of Q-values) at the diurnal and semi-diurnal periods.

We obtained a value of 0.05 μGal as the inelastic loading effect on the M_2 constituent at EGAN. On the other hand, the effect of inelasticity on the body tide is estimated at the order of 0.03 μGal from the difference between DDW_EL-HY and DDW_IE-NH (i.e. 23.976 μGal and 24.008 μGal for the former and the latter). The total inelastic effect is to be estimated at the order of 0.08 μGal at most, which is similar in magnitude to the tidal analysis error of our gravity data (see Table 3) or slightly larger than it. Therefore, unfortunately, it is difficult to constrain the inelastic effect precisely by the present analysis results, but it should be possible to measure its effect by using an updated well-calibrated stable gravimeter, better than the one used here, because of large amplitude of OTL effects in SE-AK.

Last, related to a possible source affecting the observed gravity tide, based on the tidal gravity profile obtained in Alaska (north of our study area), Zürn et al. (1976) discussed an effect of geological structure associated with the downgoing lithospheric slab beneath Alaska, and they concluded that this effect on tidal gravity perturbations will be detected when the observation and the estimation of the ocean tide effect achieve an accuracy of 0.1% and of 1%, respectively. For the ocean tide effect on M_2 constituent, Fig. 6 indicates that, for the estimation by Model B, the difference between the observation and the prediction is about 0.3 μGal and it is at the order of about 1.3% of the amplitude of predicted body tide (i.e. the ratio of 0.3–23.98 μGal). Most of the difference is considered to be due to the error in the estimation of the ocean tide effect. Therefore, improvement of the accuracy of the regional ocean tide model in SE-AK is essential for the further discussion of the tidal gravity response observed in SE-AK.

8. Conclusions

We have analyzed continuous gravity data at EGAN and GPS data at the three PBO sites AB48, AB50 and AB51 in SE-AK, and compared the observed tidal amplitudes and phases with those predicted from both the effects of body tides and ocean tides. To improve the accuracy of prediction, we also computed an improved regional ocean tide model in SE-AK. From the comparison, we obtain the conclusions as follows:

(1) For the M_2 constituent, the difference between the observed tide and the predicted one is 1% or smaller in both gravity and displacement.
(2) The PPP method works well to recover the tidal signals at the sub-centimeter accuracy or better for some tidal constituents.
(3) To accomplish the accuracy of sub-centimeter for all tidal constituents, we need to improve the accuracy of the correction for the atmospheric effects such as the tropospheric zenith delay and for the effect of multi-pass.
(4) The viscoelastic effect on the observed gravity tides is estimated to be at the order of 0.08 μGal for the M_2 tide at EGAN, as sum effect of the body tide and ocean tide. The magnitude is similar order to the analysis error for our gravity data. Increasing the accuracy of calibration of the gravimeter is needed. We also need to increase the accuracy of the regional ocean model in SE-AK.

To improve the accuracy of the regional ocean tide model, we have started the following two items: (1) the ocean bottom pressure (OBP) gauge observation has been initiated off Juneau in June 2007. We expect this observation may reveal a possible systematic modification in the existing tide gauge data obtained at the back of the narrow channel. (2) New modeling using more accurate bathymetry data than that used in this study and considering the spatial variation in the bottom friction, because of very large spatial variation in the speed of tidal currents in the sea area in SE-AK.

Acknowledgments

We acknowledge Drs. D. Inazu, K. Nakamura and T. Higuchi of the Institute of Statistical Mathematics for the discussion on ocean tide modeling. We thank Mr. T. Takasu for providing us his GPS analysis codes called "GpsTools ver. 0.6.3". Comments by three reviewers helped improve the original manuscript. We thank them for this. The ISEA project is partly supported by Grants-in-Aid for Scientific Research of MEXT of Japan: No. 17253003. US participants were supported by the National Science Foundation (NSF) grant (EAR-0408801). The temporary tide gauge data in Alaska were collected with support from NSF grant (EAR-9870144).

References

Altamimi, Z., Sillard, P., Boucher, C., 2002. ITRF2000: a new release of the International Terrestrial Reference Frame for earth science applications. J. Geophys. Res. 107 (B10), 2214, doi:10.1029/2001JB0000561.
Anderson, D.L., Given, J.W., 1982. Absorption band Q model for the Earth. J. Geophys. Res 87 (B7), 3893–3904.
Allinson, C.R., Clarke, P.J., Edwards, S.J., King, M.A., Baker, T.F., Cruddace, P.R., 2004. Stability of direct GPS estimates of ocean tide loading. Geophys. Res. Lett. 31 (15), doi:10.1029/2004GL020588.
Bock, Y., 1991. Continuous monitoring of crustal deformation. GPS World 2 (6), 40–47.
Boehm, J., Niell, A., Tregoning, P., Schuh, H., 2006. Global mapping function (GMF): a new empirical mapping function based on numerical weather model data. Geophys. Res. Lett. 33, L07304, doi:10.1029/2005GL025546.
Bos, M.S., Baker, T.F., Røthing, K., Plag, H.-P., 2002. Testing ocean tide models in the Nordic seas with tidal gravity observations. Geophys. J. Int. 150 (3), 687–694, doi:10.1046/j.1365-246X.2002.01729.x.
Choi, K., Bilich, A., Larson, K., Axelarad, P., 2004. Modified Sidereal filtering: implications for high-rate GPS positioning. Geophys. Res. Lett. 31, L22608.
Cokelet, E.D., Jenkins, A.D., Etherington, L.L., 2007. A transect of Glacier Bay ocean currents measured by accorstic Doppler current profile (ADCP). In: Piatt, J.F., Gende, S.M. (Eds.), Proceedings of the Fourth Glacier Bay Science Symposium, October 26–28, 2004, vol. 5047. U.S. Geological Survey Scientific Investigations Report, pp. 80–83.
Dehant, V., Defraigne, P., Wahr, J.M., 1999. Tides for a convective Earth. J. Geophys. Res. 104 (No. B1), 1035–1058.
Dragert, H., James, T.S., Lambert, A., 2000. Ocean loading corrections for continuous GPS: a case study at the Canadian Coastal Site Holberg. Geophys. Res. Lett. 27 (No. 14), 2045–2048.
Dziwonski, A.D., Anderson, D.L., 1981. Preliminary reference earth Model. Phys. Earth Planet. Inter. 25, 297–356.
Eanes, R.J., Bettadpur, S.V., 1994. Ocean tides from two year of TOPEX/POSEIDON altimetry. EOS Trans. AGU 75 (44), Fall Meet. (Suppl. 61).
Egbert, G.D., Bennette, A.F., Foreman, M.G.G., 1994. TOPEX/POSEIDON tides estimated using a global inverse model. J. Geophys. Res. 99 (24), 821, 824, 852.

Farrell, W.E., 1972. Deformation of the Earth by surface loads. Rev. Geophys. Space Phys. 10, 761–797.
Fujii, Y., 1967. Nmerical investigations of tidal currents in the Kurushima Straits. Bulle. Kobe Mar. Obs. 179, 1–116.
Gilbert, F., Dziewonski, A.M., 1975. An application of normal mode theory to the retrievals of structural parameters and source mechanisms from seismic spectra. Phil. Trans. R. Soc. 278A, 319–328.
Hatanaka, Y., Sengoku, A., Sato, T., Johnson, J.M., Rocken, C., Meertens, C., 2001. Detection of tidal loading signals from GPS permanent array of GSI Japan. J. Geod. Soc. Jpn. 47 (No. 1), 187–192.
Khan, S.A., Tscherning, C.C., 2001. Determination of semi-diurnal Ocean tide loading constituents using GPS in Alaska. Geophys. Res. Lett. 28 (11), 2249–2252.
King, M., 2006. Kinematic and static GPS techniques for estimating tidal displacements with application to Antarctica. J. Geodyn. 41, 77–86.
Lambert, A., Pagiatakis, S.D., Billyard, A.P., Dragert, H., 1998. Improved ocean tide loading corrections for gravity and displacement: Canada and northern United State. J. Geophys. Res. 103 (No. B12), 30231–30244.
Larsen, C.F., 2003. Rapid uplift of southern Alaska caused by recent ice loss, PhD Thesis presented to the Faculty of the University of Alaska Fairbanks.
Larsen, C.F., Motyka, R.J., Freymuller, J.T., Echelmeyer, K.A., Ivins, E.R., 2005. Rapid-viscoelastic uplift southern Alaska caused by post-Little Ice Age glacial retreat. Earth Planet. Sci. Lett. 237, 548–560.
Larsen, C.F., Motyka, R.J., Arendt, A.A., Echelmeyer, K.A., Geissler, P.E., 2007. Glacier changes in southeast Alaska and northwest British Columbia and contribution to sea level rise. J. Geophys. Res. 112, F01007, doi:10.1029/2006JF000586.
Le Provost, C., Genco, M.L., Lyard, F., Vincent, P., Canceil, P., 1994. Spectroscopy of the world ocean tides from a finite element hydrodynamic model. J. Geophys. Res. 99 (C12), 24777–24797.
Lyard, F., Lefevre, F., Letellier, T., Francis, O., 2006. Modelling the global ocean tides: modern insights from FES2004. Ocean Dyn. 56, 394–415.
Manabe, S., Sato, T., Sasaki, S., Yokoyama, K., 1991. Atmospheric loading effect on VLBI observation. In: Proceedings of the AGU Chapman Conference on Geodetic VLBI: Monitoring Global Change, AGU, pp. 111–122.
Matsumoto, K., Takanezawa, T., Ooe, M., 2000. Ocean tide models developed by assimilating TOPEX/Poseidon altimeter data into hydro-dynamical model: a global model and a regional model around Japan. J. Oceanogr. 56, 567–581.
Matsumoto, K., Sato, T., Fujimoto, H., Tamura, Y., Nishino, M., Hino, R., Higashi, T., Kanazawa, T., 2006. Ocean bottom pressure observation off Sanriku and comparison with ocean tide models, altimetry, and barotropic signals from ocean models. Geophys. Res. Lett. 33, L16602, doi:10.1029/2006GL026706.
Miura, S., Sato, T., Freymuller, J.T., Kaufman, M., Cross, R., Sun, W., Fujimoto, H., 2007. Geodetic measurements for monitoring rapid crustal uplift in southeast Alaska caused by post-glacial rebound—Outline of the project. In: Tanaka, H.L. (Ed.), Proceedings of the 7th International Conference on Global Change: Connection to Arctic (GCCA-7). International Arctic Research Center, University Alaska Fairbanks, pp. 95–97.
Neumeyer, J., del Pino, J., Dierks, O., Sun, H.P., Hartmut, P., 2005. Improvement of ocean loading correction on gravity data with additional tide gauge measurements. J. Geodyn. 40 (No. 1), 104–111.
Okubo, S., Tsuji, D., 2001. Complex Green's Function for diurnal/semidiurnal loading problem. J. Geodyn. Soc. Jpn. 47 (No. 1), 225–230.
Ray, R.D., 1999. A global ocean tide model from TOPEX/POSEIDON altimetry: GOT99.2b, Tech. Memo. 209478, NASA Goddard Space Flight Cent., Greenbelt, MD.
Sato, T., Hanada, H., 1984. A program for the computation of oceanic tidal loading effects 'GOTIC'. In: Proceedings of the International Conference on Earth Rotation and Terrest. Refer. Frame, pp. 742–747.
Sato, T., Tamura, Y., Matsumoto, K., Imanishi, Y., McQueen, H., 2004. Parameters of the fluid core resonance inferred from superconducting gravimeter data. J. Geodyn. 38, 375–389.
Schenewerk, M.S., Marshall, J., Dillinger, W., 2001. Vertical ocean-loading deformations derived from a global GPS network. J. Geodyn. Soc. Jpn. 47 (1), 237–242.
Schwiderski, E.W., 1980. On charting global ocean tides. Rev. Geophys. Space Phys. 18, 243–268.
Smith, M.L., Dahlen, F.A., 1981. The period and Q of the Chandler Wobble. Geophys. J. R. Astr. Soc. 64, 223–281.
Tamura, Y., Sato, T., Ooe, M., Ishiguro, M., 1991. A procedure for tidal analysis with a Bayesian information criterion. Geophys. J. Int. 104, 507–516.
Takasu, T., Kasai, S., 2005. Development of precise orbit/clock determination software for GPS/GNSS. In: Proceedings of the 49th Space Sciences and Technology Conference, Hiroshima, Japan (in Japanese), pp. 1223–1227.
Takasu, T., 2006. High-rate Precise Point Positioning: detection of crustal deformation by using 1-Hz GPS data. In: GPS/GNSS symposium 2006, Tokyo, pp. 52–59.
Tregoning, P., van Dam, T., 2005. Atmospheric pressure loading corrections applied to GPS data at the observation level. Geophys. Res. Lett. 32, L22310, doi:10.1029/2005GL024104.
Thomas, I.D., King, M.A., Clarke, P.J., 2007. A comparison of GPS, VLBI and model estimates of ocean tide loading displacements. J. Geodesy 81 (5),268–359.
Vey, S., Calais, E., Llubes, M., Florsch, N., Woppelmann, G., Hinderer, J., Amalvict, M., Lalancette, M.F., Simon, B., Duquenne, F., Haase, J.S., 2002. GPS measurements of ocean loading and its impact on zenith tropospheric delay estimates: a case study in Brittany, France. J. Geodyn. 76 (8), 419–427.
Wahr, J.M., 1981. Body tides of an elliptical, rotating, elastic and oceanless Earth. Geophys. R. Astron. Soc. 64, 677–703.
Zumberge, J.F., Heflin, M.B., Jefferson, D.C., Watkins, M.M., Webb, F.H., 1997. Precise point positioning for the efficient and robust analysis of GPS data from large networks. J. Geophys. Res. 102 (B3), 5005–5017.
Zürn, W., Beaumont, C., Slichter, L.B., 1976. Gravity tides and ocean loading in southern Alaska. J. Geophys. Res. 81 (No. 26), 4923–4932.